2022 IEEE 25th International Conference on Intelligent Transportation Systems (ITSC)
October 8-12, 2022, Macau, China

GNSS Outliers Mitigation in Urban Areas Using Sparse Estimation Based on Factor Graph Optimization

Xiwei Bai, Weisong Wen, Guohao Zhang, Hoi-Fung Ng, and Li-Ta Hsu*

2022 IEEE 25th International Conference on Intelligent Transportation Systems (ITSC) | 978-1-6654-6880-0/22/$31.00 ©2022 IEEE | DOI: 10.1109/ITSC55140.2022.9921906

***Abstract*— Global navigation satellite system (GNSS) plays a crucial role in providing the globally referenced positioning for self-driving systems. Unfortunately, the numerous multipath or non-line-of-sight (NLOS) receptions (known as outlier observations) caused by the signal reflections from buildings reduce the positioning accuracy of GNSS in dense urban environments. The recently investigated factor graph-based GNSS positioning formulation simultaneously considers the historical information, which significantly increases the measurement redundancy of state estimation. Taking this advantage, this paper proposes an outlier mitigation method where the bias involved in the outliers is estimated simultaneously with the position of the receiver. Specifically, the outliers are firstly detected using a pre-trained deep learning network. Secondly, an unknown variable associated with the bias is assigned to each identified outlier measurement. Then the position of the GNSS receiver, together with the bias of outlier measurements, is estimated simultaneously via the factor graph optimization (FGO) based on the pseudorange measurements and Doppler frequency shift. Finally, the effectiveness of the proposed method is validated using a dataset collected in the urban canyon by a low-cost automobile-level GNSS receiver.**

I. Introduction

With the rapid development of intelligent transportation, there has been an increasingly high demand for accurate and low-cost positioning solutions. Global navigation satellite system (GNSS) [1] is currently widely used to precisely position autonomous ground vehicles [2, 3] and unmanned aerial vehicles (UAV) [4]. However, its positioning performance in urban areas is severely degraded because GNSS measurements are contaminated by signal reflection and obstruction from nearby structures (shown in Fig. 1), resulting in multipath and non-line-of-sight (NLOS) receptions.

The mitigation of the outlier measurements has been the focus of recent research on urban GNSS positioning, and a great amount of work is being correspondingly carried out. The first attempt was to solve the problem by adding additional information, such as a 3D building model or onboard sensors. Specifically, three-dimension (3D) mapping-aided GNSS (3DMA GNSS) positioning in urban environments was employed in [5, 6]. Similarly, the 3D city model and GNSS simulator-based method were proposed to predict the bias caused by obstacles, and these biased observations were constructively applied in [7]. However, the proposed 3D city model-based method requires a 3D building model which is not always available. Interestingly, additional sensors like light detection and ranging (LiDAR) [8, 9] and camera [10] were introduced to detect and mitigate the GNSS outliers to further position autonomous systems in urban areas. Unfortunately, these methods are limited by the availability of additional sensors in practical and low-cost applications.

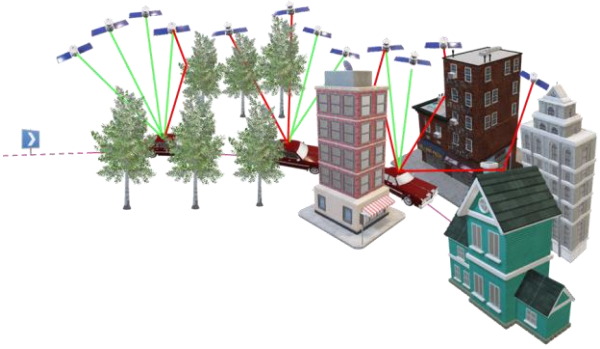

Fig. 1 An illustration of the GNSS measurements contaminated by signal reflection and obstruction from surrounding structures in an urban environment. 6 out of 12 satellites suffer reflected signals.

Thanks to available multiple satellite constellations, the number of received satellites has increased significantly, making the GNSS positioning issue even more redundant. Inspired by this fact, the work in [11] proposed a two-step GNSS positioning method with GNSS outlier bias correction. Firstly, the position of the GNSS receiver was estimated by extended Kalman filter (EKF) based on the pseudocode measurement and simplified motion model. Secondly, the bias of the potential GNSS outlier measurements was estimated based on a linearized observation matrix and measurements residuals using the least absolute shrinkage and selection operator (LASSO) [12], which is a regression analysis method. The work [11] opens a new window for research on urban GNSS positioning to explore the redundancy of multiple satellite constellations. Unfortunately, the above method has two key drawbacks: (1) The outliers were simply classified based on the final measured residuals of the EKF estimator, failing to explicitly identify the outliers. As a result, this method is not applicable in case the residuals cannot effectively indicate the outlier measurement. (2) The work [11] merely considered the measurements at a single epoch, which failed to exploit data redundancy and time-correlation from multiple epochs. Interestingly, the recently developed factor graph optimization-based GNSS positioning formulation [13] enables the simultaneous consideration of the measurements

The authors are with the Department of Aeronautical and Aviation Engineering, the Hong Kong Polytechnic University, Hong Kong. Weisong Wen is also with The Hong Kong Polytechnic University Shenzhen Research Institute, Shenzhen 518057, China. (the corresponding author to provide e-mail: lt.hsu@polyu.edu.hk).

from multiple epochs, which performs better than the EKF estimator-based GNSS positioning. A similar finding was firstly theoretically and experimentally verified in our previous work [14] where the performance of EKF on the fusion of pseudorange measurements and inertial measurement unit (IMU) was compared with that of factor graph optimization (FGO). Inspired by this, this paper proposes to fill those two key gaps by employing the deep learning network and explicitly identifying the potential GNSS outlier measurements, and increasing the measurement redundancy via the factor graphical model. Firstly, this paper exploits the potential of the deep learning network to identify the outlier measurements based on the features [15] extracted from GNSS raw measurements by our earlier work [16]. Then, based on the GNSS pseudorange and Doppler velocity measurements, the position of the GNSS receiver and the bias of the outlier measurements are simultaneously estimated via FGO, where Doppler velocity measurements are used to construct the motion connection between sequential epochs of states.

This paper is structured as follows: The method proposed in this paper is presented in Section II and elaborated in Section III. The experiments are then carried out to evaluate the performance of the proposed method in Section IV. In Section V, conclusions and future work are summarized.

II. Overview of the Proposed Method

The framework of the proposed method is depicted in Fig. 2. The system's inputs comprise the Doppler velocity measurements and raw pseudorange received by the GNSS receiver. The pseudorange measurement, as well as the position and clock bias of the satellite, are obtained by modeling the raw data. Then, in the pseudorange factor construction segment, line-of-sight (LOS) and outlier pseudorange factors are classified based on the pre-trained deep learning network (our team's prior work [16]), in which GNSS features such as azimuth, elevation angles were extracted with the help of preprocessing the raw data. Furthermore, the Doppler factor is derived by modeling the Doppler measurements. Finally, by resolving the factor graph formulation formed by the pseudorange and Doppler factors, the state estimation of the GNSS receiver is derived. More specifically, the pseudorange factor involves LOS and outlier pseudorange factors.

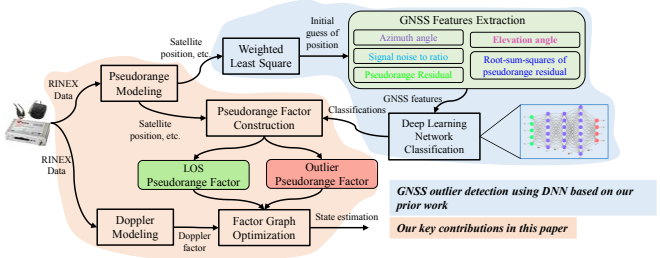

Fig. 2 The framework of the method presented in this paper.

The contribution of this paper is listed as follows:

(1) The method presented in this paper aims to mitigate the impacts of the outliers by estimating the position of the GNSS receiver and the potential bias of outlier measurements based on FGO, where the GNSS outlier measurements are identified using the deep learning-based network.

(2) The reliable estimation of the bias associated with the outliers strongly depends on the redundancy of healthy measurements. To guarantee the redundancy of measurements, we propose to estimate bias using the sparse estimation method, where factor graph-based GNSS positioning formulation is employed to simultaneously integrate the historical information from multiple epochs.

III. Methodology

The methodology of the GNSS outliers mitigation is explained in this section. Specifically, the Doppler frequency measurements are utilized to provide velocity constraints between sequential epochs, and the Doppler frequency shift and pseudorange measurements are loosely coupled (LC) integrated based on FGO. The global positioning system (GPS) and BeiDou satellite system are used in this paper. The GNSS receiver is represented by r. The set of states $\boldsymbol{\chi}$ of the GNSS receiver is denoted as:

$$\boldsymbol{\chi} = [\mathbf{x}_{r,1}, \mathbf{x}_{r,2}, \dots, \mathbf{x}_{r,n}] \tag{1}$$

$$\mathbf{x}_{r,t} = (\mathbf{p}_{r,t}, \mathbf{v}_{r,t}, \delta_{r,t}, b_{r,t}^{1,o}, b_{r,t}^{2,o}, \dots, b_{r,t}^{s,o})^T \tag{2}$$

where each bold letter $\mathbf{x}$ denotes the state of GNSS receiver r at different epochs. The subscript n indicates the total epochs of observations considered in FGO. The $\mathbf{x}_{r,t}$ represents the receiver's state at epoch t, $t \in (1, n)$, which involves the position $\mathbf{p}_{r,t}(x_{r,t}, y_{r,t}, z_{r,t})$, velocity $(\mathbf{v}_{r,t})$ and receiver clock bias $(\delta_{r,t})$. For the sake of simplicity, we only describe the receiver clock bias for one of the satellite constellations (GPS, Beidou). $b_{r,t}^{s,o}$ denotes the bias associated with the detected outliers. The superscripts s and o denote the index of satellites and the identified outliers, respectively.

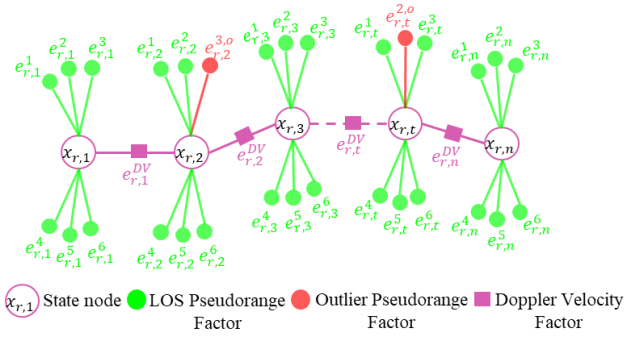

Fig. 3 The proposed FGO structure for GNSS positioning. The estimated state of the receiver is represented by the purple circle, the LOS pseudorange factor by the green shaded circle, and the pseudorange factor from the contaminated satellites depicted in Fig. 1 by the red circle.

The structure of the proposed GNSS-based positioning factor graph is illustrated in Fig. 3. The purple circle denotes the state node $\mathbf{x}_{r,t}$ of the receiver, and n is the total of epochs utilized in the optimization. The state nodes in the factor graph are connected using the Doppler velocity factor, each consisting of the LOS pseudorange factors as well as the

outlier pseudorange factor. Our proposed method makes use of the sparsity of outlier pseudorange measurements to estimate the bias based on the graph structure.

A. Pseudorange Measurement Modeling

The raw measurements are provided by the GNSS receiver, and the pseudorange measurement for a specific satellite s at epoch t is defined as follows [17].

$$\rho_{r,t}^{s} = r_{r,t}^{s} + c\left(\delta_{r,t} - \delta_{r,t}^{s}\right) + I_{r,t}^{s} + T_{r,t}^{s} + b_{r,t}^{s,o} + \varepsilon_{r,t}^{s} \quad (3)$$

where $r_{r,t}^{s}$ denotes the geometric distance from the satellite s to the GNSS receiver r at epoch t. c denotes the speed of the light. $\delta_{r,t}^{s}$ denotes the clock bias of satellite. $I_{r,t}^{s}$ and $T_{r,t}^{s}$ represent ionospheric and tropospheric delay distances, respectively, and they are modeled following the method in [18]. $b_{r,t}^{s,o}$ indicates the bias mentioned in (2), and the associated outliers depends on the identification of deep learning network. Concretely, if the satellite s is classified as healthy, then the bias equals 0. Otherwise, the value of bias is associated with the detected outliers. The details of the identification of outliers are given in Algorithm 1. Besides, the effects of errors caused by multipath and NLOS receptions and system errors (e.g receiver noise) are expressed by $\varepsilon_{r,t}^{s}$.

Before constructing the observation model, we recall the principles of outlier identification by the deep learning network employed in this paper, which is one of our previous works [16]. The input of the deep learning network was extracted from brief representations including elevation and azimuth angles, carrier-to-noise density ratio (C/N_0), individual pseudorange residual and the root-sum-squares of pseudorange residuals from all available satellites. Satellite visibility was intimately related to these GNSS features, and pseudorange residuals were highly dependent on the environment. To effectively model the network, the features were extracted from the preprocessed data. The preprocessed data were obtained by solving the weighted least squares, as shown in Fig. 2. Then, the deep learning network output the predicted visibility value of satellites ($p^{s,v}$) and predicted pseudorange error ($\rho^{s,e}$). Besides, the proposed network integrated conventional fully connected neural networks (FCNNs) and long short-term memory (LSTM) networks. More details about the designed network are presented in our prior work [16].

The details of the algorithm used to identify the outlier are seen in Algorithm 1. The algorithm's inputs are $p^{s,v}$ and $\rho^{s,e}$. Besides, the research [19] shows that C/N_0 also can describe signal strength, and thus is introduced to the algorithm, denoted by s^{CN_0}. T^{CN_0} denotes the minimum received signal strength. $\mathrm{T}^{s,v}$ and $\mathrm{T}^{s,e}$ are the thresholds set for visibility value and pseudorange error to be experimentally determined.

Based on the classification of visibility, the observation model for the LOS pseudorange measurements of a specific satellite s is stated as:

$$\rho_{r,t}^{s} = h_{r,t}^{s}\left(\mathbf{p}_{r,t}, \mathbf{p}_{t}^{s}, \delta_{r,t}\right) + \omega_{r,t}^{s} \quad (4)$$

$$\text{with } h_{r,t}^{s}\left(\mathbf{p}_{r,t}, \mathbf{p}_{t}^{s}, \delta_{r,t}\right) = ||\mathbf{p}_{t}^{s} - \mathbf{p}_{r,t}|| + \delta_{r,t}$$

where the position of the satellite at epoch t is indicated by $\mathbf{p}_{t}^{s}$ and that of the receiver by $\mathbf{p}_{r,t}$. The noise represented by $\omega_{r,t}^{s}$ is assumed to be Gaussian white noise, $\omega_{r,t}^{s} \sim \mathcal{N}(0, \Sigma_{r,t}^{s})$. $\Sigma_{r,t}^{s}$ denotes the covariance for the given satellite s. Therefore, the error function $\mathrm{e}_{r,t}^{s}$ for a given measurement $\rho_{r,t}^{s}$ can be derived as:

$$||\mathrm{e}_{r,t}^{s}||_{\Sigma_{r,t}^{s}}^{2} = ||\rho_{r,t}^{s} - h_{r,t}^{s}\left(\mathbf{p}_{r,t}, \mathbf{p}_{t}^{s}, \delta_{r,t}\right)||_{\Sigma_{r,t}^{s}}^{2} \quad (5)$$

where the covariance $\Sigma_{r,t}^{s}$ is obtained based on the elevation angle and C/N_0 of the satellite. The details are given in [20].

Algorithm 1: Identification of outlier satellite

Input: The predicted visibility value $p^{s,v}$, the predicted pseudorange error $\rho^{s,e}$, the corresponding C/N_0 of the satellite

Output: The outlier $\rho_{r,t}^{s,o}$ and the LOS measurement $\rho_{r,t}^{s}$

Step1: To identify the outlier satellite based on the $p^{s,v}$, $\rho^{s,e}$ and s^{CN_0} of the satellite are:

$$p^{s,v} < \mathrm{T}^{s,v} \quad (6)$$

$$\rho^{s,e} > \mathrm{T}^{s,e} \quad (7)$$

If the predicted visibility value and pseudorange error of the satellite satisfy the above conditions (6) and (7) simultaneously, then the satellite is identified as an outlier, otherwise, it is identified as LOS.

Step2: The signal strength information is employed to further distinguish potential outliers from the LOS identified based on Step 1 as follows:

$$s^{CN_0} < \mathrm{T}^{CN_0} \quad (8)$$

If the s^{CN_0} associated with the identified LOS is smaller than T^{CN_0}, then the satellite is identified as an outlier, otherwise, it is identified as LOS.

The observation model of the outlier measurement is formulated as:

$$\rho_{r,t}^{s,o} = h_{r,t}^{s,o}\left(\mathbf{p}_{r,t}, \mathbf{p}_{t}^{s,o}, \delta_{r,t}, b_{r,t}^{s,o}\right) + \omega_{r,t}^{s,o} \quad (9)$$

$$\text{with } h_{r,t}^{s,o}\left(\mathbf{p}_{r,t}, \mathbf{p}_{t}^{s,o}, \delta_{r,t}, b_{r,t}^{s,o}\right) = ||\mathbf{p}_{t}^{s,o} - \mathbf{p}_{r,t}|| + b_{r,t}^{s,o} + \delta_{r,t}$$

where the bias concerning the identified outlier is indicated by $b_{r,t}^{s,o}$ and the noise represented by $\omega_{r,t}^{s,o}$ is also assumed to be Gaussian white noise, $\omega_{r,t}^{s,o} \sim \mathcal{N}(0, \Sigma_{r,t}^{s,o})$. $\Sigma_{r,t}^{s,o}$ denotes the covariance for the outlier satellite. The error function $\mathrm{e}_{r,t}^{s,o}$ for the outlier measurement $\rho_{r,t}^{s,o}$ is then derived as:

$$||\mathrm{e}_{r,t}^{s,o}||_{\Sigma_{r,t}^{s,o}}^{2} = ||\rho_{r,t}^{s,o} - h_{r,t}^{s,o}\left(\mathbf{p}_{r,t}, \mathbf{p}_{t}^{s,o}, \delta_{r,t}, b_{r,t}^{s,o}\right)||_{\Sigma_{r,t}^{s,o}}^{2} \quad (10)$$

where $\Sigma_{r,t}^{s,o}$ is obtained in the same way as $\Sigma_{r,t}^{s}$, which is based on the elevation angle and C/N_0 of the outlier satellite [20].

B. Doppler Velocity Measurement Modeling

The measured velocity can be calculated based on the weighted least square method [21]. The observation model for the Doppler velocity measurement is expressed as:

$$\mathbf{v}_{r,t}^{DV} = h_{r,t}^{DV}\left(\mathbf{x}_{r,t+1}, \mathbf{x}_{r,t}\right) + \boldsymbol{\omega}_{r,t}^{DV} \tag{11}$$

$$\text{with } h_{r,t}^{DV}\left(\mathbf{x}_{r,t+1}, \mathbf{x}_{r,t}\right) = \begin{bmatrix} \left(x_{r,t+1} - x_{r,t}\right)/\Delta t \\ \left(y_{r,t+1} - y_{r,t}\right)/\Delta t \\ \left(z_{r,t+1} - z_{r,t}\right)/\Delta t \end{bmatrix}$$

where the velocity measurement is represented by $\mathbf{v}_{r,t}^{DV}$. The noise represented by $\boldsymbol{\omega}_{r,t}^{DV}$ is also assumed to be Gaussian white noise, $\boldsymbol{\omega}_{r,t}^{DV} \sim \mathcal{N}(0, \boldsymbol{\Sigma}_{r,t}^{DV})$. $\boldsymbol{\Sigma}_{r,t}^{DV}$ denotes the covariance matrix for $\mathbf{v}_{r,t}^{DV}$. The states of the receiver at consecutive epochs t and $t+1$ are individually represented by $\mathbf{x}_{r,t}$ and $\mathbf{x}_{r,t+1}$. Δt denotes the time difference between the two consecutive states. Thus, the error function for a given velocity measurement is derived as:

$$||\mathbf{e}_{r,t}^{DV}||_{\boldsymbol{\Sigma}_{r,t}^{DV}}^2 = ||\frac{\mathbf{v}_{r,t}^{DV} + \mathbf{v}_{r,t+1}^{DV}}{2} - h_{r,t}^{DV}\left(\mathbf{x}_{r,t+1}, \mathbf{x}_{r,t}\right)||_{\boldsymbol{\Sigma}_{r,t}^{DV}}^2 \tag{12}$$

C. GNSS Positioning Using Factor Graph Optimization

The objective function of the GNSS positioning problem based on FGO can be expressed as:

$$\boldsymbol{\chi}^* = \arg\min_{\boldsymbol{\chi}} \sum_{s,t} ||\mathbf{e}_{r,t}^{DV}||_{\boldsymbol{\Sigma}_{r,t}^{DV}}^2 + ||\mathbf{e}_{r,t}^{s}||_{\boldsymbol{\Sigma}_{r,t}^{s}}^2 + ||\mathbf{e}_{r,t}^{s,o}||_{\boldsymbol{\Sigma}_{r,t}^{s,o}}^2 \tag{13}$$

By resolving the objective function, the optimal estimation of the sets of states represented by $\boldsymbol{\chi}^*$ can be derived. Meanwhile, Ceres [22] is used as the nonlinear optimization solver.

IV. Experimental Results and Discussion

Experimental scenario: The experiment data was collected in an urban canyon in Hong Kong. Fig. 4-(a) and (b) show the experimental trajectory and corresponding urban scenario, respectively. As shown in Fig. 4-(b), lots of tall buildings located on both sides of the road introduced lots of challenges to the GNSS positioning.

Sensor setup: In this experiment, a u-blox M8T automobile-level GNSS receiver was employed to collect satellite (GPS/BeiDou) observations at a frequency of 1 Hz. To evaluate the improved performance of the proposed method, the ground truth of positioning was provided by a NovAtel SPAN-CPT inertial navigation system. To guarantee the accuracy and reliability of the ground truth, the data from SPAN-CPT was post-processed using the inertial explorer software from NovAtel. The timestamp of collected data was synchronized in a robot operation system (ROS) [23]. The setup of the sensor used in this paper is introduced in more detail in our recently open-sourced UrbanNav dataset [24].

More specifically, the processor of our laptop computer used for evaluating the positioning performance was Intel Core i7-9750H CPU @2.60GHz and 16.0 GB RAM. To validate the effectiveness of the proposed method, we compared the following methods:

(1) **FGO**: GNSS positioning by LC integration of Doppler velocity measurements and pseudorange measurements based on FGO [13].

(2) **FGO-DL-Outliers (the proposed method)**: The effects of GNSS outliers are mitigated by LC integration of Doppler velocity measurements and pseudorange measurements based on FGO. Meanwhile, the outliers are identified by the trained deep learning (DL) network [16]. The bias state involved in the outliers is then estimated simultaneously with the position of the receiver.

The positioning accuracy of the above two methods was evaluated under the local east-north-up (ENU) coordinate system. Due to the geometric distribution of satellites, the GNSS positioning in the upward direction was not ideal, so only the positioning accuracy in the eastern and northern directions was evaluated.

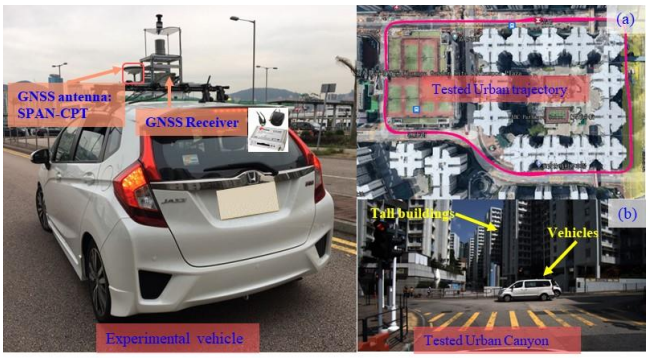

Fig. 4 The experimental setups are shown in the left figure. The trajectory and experimental scenario are shown in Fig. 4-(a) and (b).

A. Experimental Evaluation in an Urban Canyon

Table 1 displays the GNSS positioning errors for the two methods mentioned above. Based on FGO LC integration of pseudorange and Doppler velocity measurements, the mean positioning error was 10.03 meters, and the maximum positioning error was even up to 22.84 meters. With the aid of the proposed method FGO-DL-Outliers, the mean error dramatically decreased to 8.67 meters with the standard deviation (STD) of 3.89 meters. The mean positioning error made by the proposed method was reduced by about 13.5% compared to that made by the FGO method. The trajectories of the two listed methods and ground truth are shown in Fig. 5. The ground truth was provided by the SPAN-CPT. Compared to the FGO method, the overall trajectory of FGO-DL-Outliers was closer to the ground truth. Fig. 6 shows the mean errors of the listed two methods. As can be seen from the figure, the mean error of the proposed method (blue curve) dramatically dropped from 10.03 meters to 8.67 meters, revealing that the proposed method could help to reduce the impact of the outlier measurement on the used dataset.

Table.1 The GNSS positioning error based on the two listed methods

Item	FGO	FGO-DL-Outliers	Improvement
Mean (m)	10.03	8.67	13.5%
STD (m)	4.70	3.89	17.2%
Max (m)	22.84	30.39	

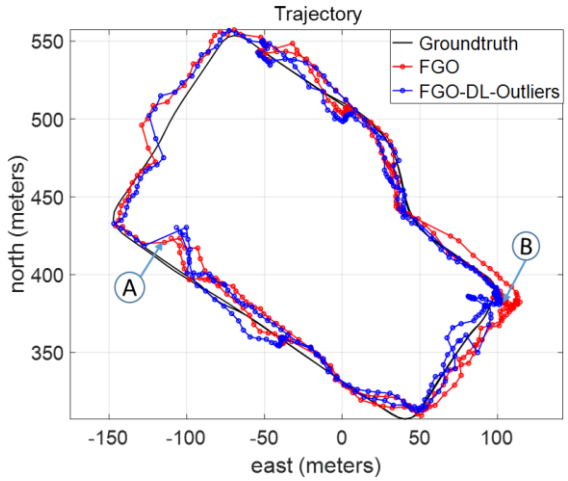

Fig. 5 The trajectories of the two methods FGO (red) and FGO-DL-Outliers (blue). The ground truth is shown in the black curve. The x-axis and y-axis denote east and north directions, respectively.

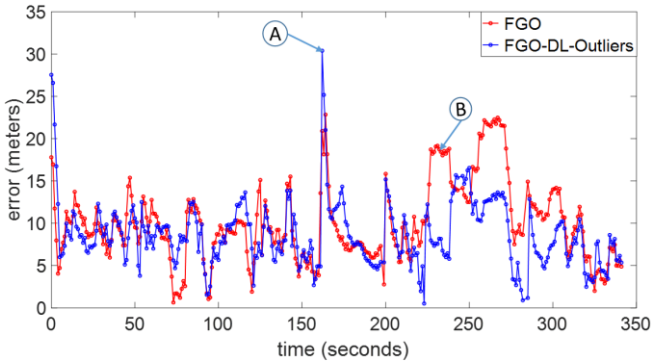

Fig. 6 The mean error of the two listed methods: FGO (red), and FGO-DL-Outliers (blue).

Interestingly, the maximum error conversely increased from 22.84 meters (FGO) to 30.39 meters using the proposed method, corresponding to epoch "A" in Fig. 6. Conversely, a great improvement can be seen in epoch "B", as the error decreased from 18 meters to 6.76 meters with the help of the proposed method. To explore the underlying reason, the number of outlier satellites and the total number of satellites are shown in Fig. 7, respectively. The more detailed information on the number of satellites at epochs "A" and "B" is further displayed in Fig. 8.

To further show the results of the outlier detected using the proposed method, we labeled the ground truth of the satellite visibility using the 3D building model based on our previous work in [25]. Meanwhile, the satellite visibility at epoch "A" and epoch "B" is shown in Fig. 8 via skyplot [25]. Specifically, the gray shaded area represents the non-sky area (potentially blocked by buildings) and the white area represents the sky area. The different circles in the skyplot denote different elevation angles with a resolution of 10 degrees. The satellite located within the non-sky area is the NLOS (red shaded circle) and vice versa.

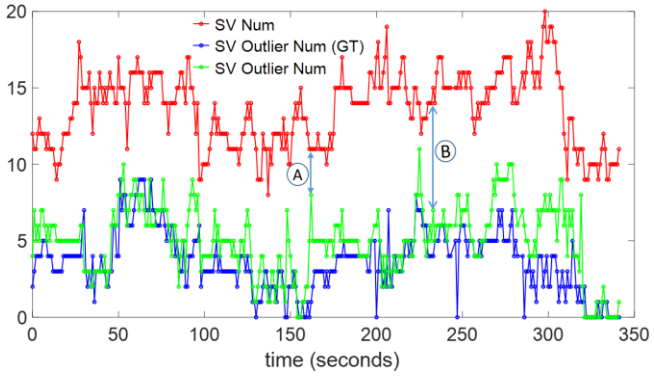

Fig. 7 The total number of satellites and the number of outlier satellites. The total number of satellites at each epoch is denoted by the red curve, the number of outlier satellites by the blue curve, and the number of the outlier satellites predicted by the deep learning network by the green curve.

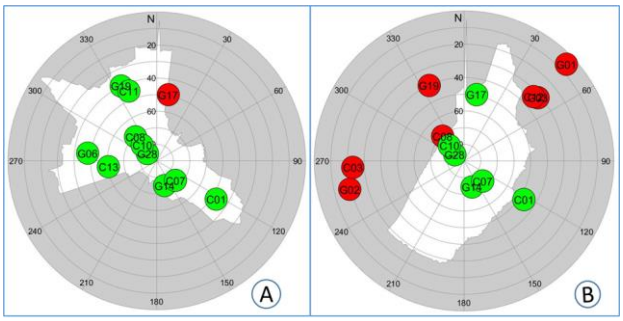

Fig. 8 The skyplot corresponds to epochs "A" and "B". The red shaded circle denotes the outliers, and the green shaded circle denotes the healthy satellites. The outliers shown in the skyplot are labeled by a 3D building model as ground truth.

At epoch "A", the total number of satellites received by the GNSS receiver was 11. The exact number of outliers was 1, which was labeled by the 3D building model as ground truth. However, 8 outliers were predicted by the deep learning network. Therefore, it can be concluded that the positioning error increased significantly at this epoch due to the limited redundancy of measurements. Additionally, limited measurement redundancy was caused by healthy measurements misidentified as outliers.

At epoch "B", the total number of satellites was 13, and the exact number of outlier satellites was 7, which was labeled by the 3D building model as ground truth. The number of the predicted outlier measurements was the same as the ground truth, with the measurement redundancy at this epoch. Therefore, the positioning performance at epoch "B" was improved.

V. Conclusion and Future Work

The outliers mitigation method based on FGO was proposed for GNSS positioning in this research, where the

outlier measurements were first identified using the deep learning network and then the bias associated with the outlier measurements was estimated together with the state of the GNSS receiver simultaneously.

The effectiveness of the proposed method was preliminarily validated in urban Hong Kong. According to the preliminary result, the impacts of GNSS outlier measurement were mitigated for further GNSS positioning. However, the improved performance of the proposed method is limited by bound measurement redundancy. In other words, an intelligent transportation system remains a challenge in urban areas.

Moreover, the same uncertainties were assigned to the healthy LOS and outlier GNSS measurements although the additional bias for the outlier measurements was estimated. Therefore, we intend to explore the adaptive covariance matrix for potential GNSS outlier measurements and verify our proposed method by using more data collected in urban environments in future work.

ACKNOWLEDGMENT

This work is financially supported by the Research Impact Fund Scheme under Hong Kong University Grants Committee. The project title is “Reliable Multiagent Collaborative Global Navigation Satellite System Positioning for Intelligent Transportation Systems” and the project reference number is “R5009-21”. This research is also supported by Guangdong Natural Science Foundation (2021A1515110771). Besides, this work is partially supported by Hong Kong PolyU Startup Fund through the Resilient GNSS Positioning for Autonomous Aerial Vehicle in Urban Scenarios. The project reference number is “BD63”.

REFERENCES

[1] J. Meguro, T. Arakawa, S. Mizutani, and A. Takanose, "Low-cost lane-level positioning in urban area using optimized long time series GNSS and IMU data", *2018 21st International Conference on Intelligent Transportation Systems (ITSC)*, 2018: IEEE, pp. 3097-3104.

[2] G. Wan *et al.*, "Robust and precise vehicle localization based on multi-sensor fusion in diverse city scenes", *2018 IEEE International Conference on Robotics and Automation (ICRA)*, 2018: IEEE, pp. 4670-4677.

[3] Y. Zein, M. Darwiche, and O. Mokhiamar, "GPS tracking system for autonomous vehicles", *Alexandria engineering journal,* vol. 57, no. 4, pp. 3127-3137, 2018.

[4] A. Al-Kaff, R. Alonso, M. Osman, and A. Hussein, "Skyonyx: Autonomous uav research platform for air transportation system (atsys)", *2018 21st International Conference on Intelligent Transportation Systems (ITSC)*, 2018: IEEE, pp. 3550-3555.

[5] L.-T. Hsu, Y. Gu, and S. Kamijo, "3D building model-based pedestrian positioning method using GPS/GLONASS/QZSS and its reliability calculation" (in English), *GPS Solutions,* vol. 20, no. 3, pp. 413–428, 2016. [Online]. Available: http://dx.doi.org/10.1007/s10291-015-0451-7.

[6] Q. Zhong and P. D. Groves, "Multi-Epoch 3D-Mapping-Aided Positioning using Bayesian Filtering Techniques", *Proceedings of the 34th International Technical Meeting of the Satellite Division of The Institute of Navigation (ION GNSS+ 2021)*, 2021, pp. 195-225.

[7] N. Kbayer, M. J. I. T. o. A. Sahmoudi, and E. Systems, "Performances analysis of GNSS NLOS bias correction in urban environment using a three-dimensional city model and GNSS simulator", vol. 54, no. 4, pp. 1799-1814, 2018.

[8] W. Wen, G. Zhang, and L. T. Hsu, "Correcting NLOS by 3D LiDAR and building height to improve GNSS single point positioning", *Navigation,* vol. 66, no. 4, pp. 705-718, 2019.

[9] W. Wen, "3D LiDAR aided GNSS and its tightly coupled integration with INS via factor graph optimization", *Proceedings of the 33rd International Technical Meeting of the Satellite Division of The Institute of Navigation (ION GNSS+ 2020)*, 2020, pp. 1649-1672.

[10] X. Bai, W. Wen, and L.-T. Hsu, "Using Sky-pointing fish-eye camera and LiDAR to aid GNSS single-point positioning in urban canyons", *IET Intelligent Transport Systems,* vol. 14, no. 8, pp. 908-914, 2020.

[11] J. Lesouple, T. Robert, M. Sahmoudi, J.-Y. Tourneret, and W. Vigneau, "Multipath mitigation for GNSS positioning in an urban environment using sparse estimation", *IEEE Transactions on Intelligent Transportation Systems,* vol. 20, no. 4, pp. 1316-1328, 2018.

[12] S. L. Kukreja, J. Löfberg, and M. J. Brenner, "A least absolute shrinkage and selection operator (LASSO) for nonlinear system identification", *IFAC proceedings volumes,* vol. 39, no. 1, pp. 814-819, 2006.

[13] W. Wen and L.-T. Hsu, "Towards robust GNSS positioning and Real-time kinematic using factor graph optimization", *2021 IEEE International Conference on Robotics and Automation (ICRA)*, 2021: IEEE, pp. 5884-5890.

[14] W. Wen, T. Pfeifer, X. Bai, and L.-T. Hsu, "Factor graph optimization for GNSS/INS integration: A comparison with the extended Kalman filter", *NAVIGATION, Journal of the Institute of Navigation,* vol. 68, no. 2, pp. 315-331, 2021.

[15] L.-T. Hsu, "GNSS multipath detection using a machine learning approach", *2017 IEEE 20th International Conference on Intelligent Transportation Systems (ITSC)*, 2017: IEEE, pp. 1-6.

[16] G. Zhang, P. Xu, H. Xu, and L.-T. Hsu, "Prediction on the Urban GNSS Measurement Uncertainty Based on Deep Learning Networks With Long Short-Term Memory", *IEEE Sensors Journal,* vol. 21, no. 18, pp. 20563-20577, 2021.

[17] E. Kaplan and C. Hegarty, *Understanding GPS: principles and applications*. Artech house, 2005.

[18] T. Takasu and A. Yasuda, "Development of the low-cost RTK-GPS receiver with an open source program package RTKLIB", *International symposium on GPS/GNSS*, 2009: International Convention Center Jeju Korea, pp. 4-6.

[19] C. Rost and L. Wanninger, "Carrier phase multipath mitigation based on GNSS signal quality measurements", 2009.

[20] A. M. Herrera, H. F. Suhandri, E. Realini, M. Reguzzoni, and M. C. de Lacy, "goGPS: open-source MATLAB software", *Gps Solut,* vol. 20, no. 3, pp. 595-603, 2016, doi: https://doi.org/10.1007/s10291-015-0469-x.

[21] B. Hofmann-Wellenhof, H. Lichtenegger, and E. Wasle, *GNSS–global navigation satellite systems: GPS, GLONASS, Galileo, and more*. Springer Science & Business Media, 2007.

[22] S. Agarwal and K. Mierle, "Ceres solver", 2012.

[23] M. Quigley *et al.*, "ROS: an open-source Robot Operating System", *ICRA workshop on open source software*, 2009, vol. 3, no. 3.2: Kobe, Japan, p. 5.

[24] L.-T. Hsu *et al.*, "UrbanNav: An open-sourced multisensory dataset for benchmarking positioning algorithms designed for urban areas", *Proceedings of the 34th International Technical Meeting of the Satellite Division of The Institute of Navigation (ION GNSS+ 2021)*, 2021, pp. 226-256.

[25] H.-F. Ng, G. Zhang, and L.-T. Hsu, "A computation effective range-based 3D mapping aided GNSS with NLOS correction method", *The Journal of Navigation,* vol. 73, no. 6, pp. 1202-1222, 2020.